

# Nondimensional representations for occulter design and performance evaluation

Eric Cady

Jet Propulsion Laboratory, California Institute of Technology, Pasadena, CA, 91109 USA

## ABSTRACT

An occulter is a spacecraft with a precisely-shaped optical edges which flies in formation with a telescope, blocking light from a star while leaving light from nearby planets unaffected. Using linear optimization, occulters can be designed for use with telescopes over a wide range of telescope aperture sizes, science bands, and starlight suppression levels. It can be shown that this optimization depends primarily on a small number of independent nondimensional parameters, which correspond to Fresnel numbers and physical scales and enter the optimization only as constraints. We show how these can be used to span the parameter space of possible optimized occulters; this data set can then be mined to determine occulter sizes for various mission scenarios and sets of engineering constraints.

## 1. INTRODUCTION

The challenges of imaging planets like Earth around other stars come from two areas: angular resolution and contrast. An Earth-mass planet around a Sun-like star 10 parsecs will be 100 milliarcseconds from the star, and  $10^{10}$  times dimmer in visible light. The difficulty of resolving such a faint object at such a small angular separation has pushed the development of a number of technologies with the capability of meeting this challenge, one of which is the use of an occulter.

An occulter is a spacecraft which is flown in front of a telescope to block starlight while letting the light on nearby planets through. Careful shaping of the edge controls diffraction from the occulter, allowing the star to be nulled by a factor  $10^{10}$  or more over a broad spectral band, while the finite angular size means that nearby planets (with separations on the order of 100mas) will not be affected. These spacecraft are tens of meters in diameter and fly tens of thousands of kilometers from the telescope; a diagram of a typical system is shown in Fig. 1. The exact values of size, distance, angular size, and wavelengths of operation are variables that go into the design of an occulter, and many of these choices are degenerate—for example, some choices of bandpass and distance will produce the same occulter shape.

In this paper, we online a framework for removing these degeneracies and spanning the parameter space of potential occulter designs. We do this by reducing the propagation equations to dependence on a smaller number of independent nondimensional parameters; the process for this is described in § 2. IN § 3, we use

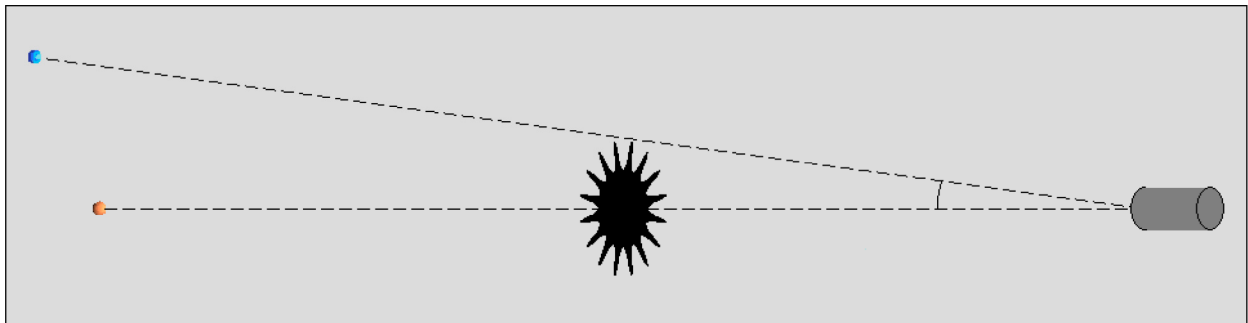


Figure 1. A typical occulter system, allowing planet light (from the blue source) to pass the edge of the occulter while blocking starlight.

these parameters to populate a grid of suppression data, and to extract information about the limits of occulter performance under various engineering and science constraints.

## 2. PROPAGATION EQUATIONS

To begin, we write the electric field at the telescope pupil in terms of system parameters:  $R$ , the occulter radius;  $\lambda$ , the wavelength under consideration; and  $z$ , the distance from telescope to occulter. As shown in,<sup>1</sup> this can be written as:

$$\begin{aligned}
 E_{\text{occ}}(\rho, \phi; \lambda) = & E_0 e^{2\pi iz/\lambda} \left( 1 - \frac{2\pi}{i\lambda z} \int_0^R A(r) J_0 \left( \frac{2\pi r \rho}{\lambda z} \right) e^{\frac{\pi i}{\lambda z} (r^2 + \rho^2)} r dr \right) \\
 & - E_0 e^{2\pi iz/\lambda} \sum_{j=1}^{\infty} \frac{(-1)^j 2\pi}{i\lambda z} \left( \int_0^R e^{\frac{\pi i}{\lambda z} (r^2 + \rho^2)} J_{jN} \left( \frac{2\pi r \rho}{\lambda z} \right) \frac{\sin(j\pi A(r))}{j\pi} r dr \right) \\
 & \times (2 \cos(jN(\phi - \pi/2)))
 \end{aligned} \tag{1}$$

where  $N$  is the number of petals on the occulter and  $(r, \theta)$  and  $(\rho, \phi)$  are polar coordinates at the occulter and telescope planes, respectively.  $A(r)$  is the shape profile which defines the occulter, and it is defined so that if a circle of radius  $r$  is drawn under the occulter, the fraction blocked by the occulter is  $A(r)$ . Generally,  $A(r) = 1$  for all  $r < a < R$ ; this creates a solid central disk of radius  $a$  which provides a location for the spacecraft bus to be placed.

The ranges of the variables and parameters are constrained by the design of the system.  $\rho$  is allowed to vary between 0 and  $\rho_{\text{max}}$ , which we define as the sum of the radius of the telescope and our chosen tolerance for lateral alignment of the occulter. As the occulter must work over a broad band,  $\lambda$  will be allowed to vary freely between  $\lambda_{\text{min}}$  and  $\lambda_{\text{max}}$ . To avoid any wavelength-dependent transmission effects, and to reduce the tolerancing requirements, we set the inner working angle (IWA) to the angle subtended geometrically by the occulter:  $IWA \approx R/z$ , corresponding to its angular radius on the sky.

For points close to the optical axis and sufficiently large  $N$ , it is reasonable to consider only the first,  $\phi$ -independent term of Eq. 1, as the remaining terms in the series will be negligibly small. For this reason, we use the following approximation to Eq. 1 when designing occulters:

$$E_{\text{apod}}(\rho; \lambda) = E_0 e^{2\pi iz/\lambda} \left( 1 - \frac{2\pi}{i\lambda z} \int_0^R A(r) J_0 \left( \frac{2\pi r \rho}{\lambda z} \right) e^{\frac{\pi i}{\lambda z} (r^2 + \rho^2)} r dr \right) \tag{2}$$

We design occulters using an optimization on  $A(r)$ ;<sup>1,2</sup> using Eq. 2 in place of Eq. 1 allows the optimization to remain linear, which produces globally-optimal solutions. Subsequent simulations of propagation, as well as all tolerancing, are done with the full Eq. 1.

### 2.1 Nondimensionalization

The integrals in Eq. 1 and Eq. 2 are invariant under certain transformations to within a constant phase factor; for example, replacing  $z$  by  $zc$  and  $\lambda$  by  $\lambda/c$  leaves these integrals unchanged (except for the constant  $e^{2\pi iz/\lambda}$ , which is of magnitude 1 and does not affect the measured intensity). Many approaches to occulters have taken advantage of these useful scaling properties. Two-distance occulters such as THEIA<sup>3</sup> and O<sub>3</sub><sup>4</sup> use the  $z \rightarrow zc, \lambda \rightarrow \lambda/c$  transformation to allow them to extend their capability into the near infrared, at the cost of inner working angle. Occulter laboratory experiments<sup>5-9</sup> scale their radius and distance by  $r \rightarrow r/c, \rho \rightarrow \rho/c, z \rightarrow z/c^2$  to allow occulters to be investigated at the laboratory scale.

We can remove this degeneracy in the propagation equation, and eliminate all explicit dependence on these degenerate parameters, by nondimensionalizing the parameters. This allows us to succinctly span the phase space of occulter designs with four nondimensional independent parameters\*, defined as:

---

\*It is possible to introduce additional parameters, e.g. constraints on sizes of petal tips and gaps or wavelength-dependent weightings. Generally, however, these will have smaller effects, and we will only consider these four for the purposes of this analysis.

Parameter	Definition	Description
$N_1$	$\frac{R^2}{\lambda_{\max} z} = \frac{R \times IWA}{\lambda_{\max}}$	maximum-wavelength occulter Fresnel number
$N_2$	$\frac{R^2}{\lambda_{\min} z} = \frac{R \times IWA}{\lambda_{\min}}$	minimum-wavelength occulter Fresnel number
$N_3$	$\frac{\rho_{\max}^2}{\lambda_{\max} z}$	maximum-wavelength shadow Fresnel number
$N_4$	$\frac{a}{R}$	ratio of central disk radius to full radius

Table 1. The set of nondimensional parameters chosen to bound an optimization.

If we define some new nondimensional lengths and Fresnel numbers:

$$r' \equiv \frac{r}{R}, 0 \leq r' \leq 1 \quad (3)$$

$$\rho' \equiv \frac{\rho}{\rho_{\max}}, 0 \leq \rho' \leq 1 \quad (4)$$

$$N_o \equiv \frac{r^2}{\lambda z} \quad (5)$$

$$N_t \equiv \frac{\rho^2}{\lambda z} A'(r') = A(r) \quad (6)$$

then Eq. 2 can be rewritten as:

$$E(\rho'; N_o, N_t) = 1 + 2\pi i N_o \int_0^1 A'(r') J_0 \left( 2\pi \sqrt{N_o N_t} r' \rho' \right) e^{\pi i (N_o r'^2 + N_t \rho'^2)} r' dr' \quad (7)$$

$N_1$ ,  $N_2$ ,  $N_3$ , and  $N_4$  only enter as bounds; the optimization finds an  $A'(r')$  which minimizes  $E(\rho')$  between these bounds subject to

$$N_1 \leq N_o \leq N_2 \quad (8)$$

$$N_3 \leq N_t \leq \frac{N_3 N_2}{N_1} \quad (9)$$

$$A'(r') = 1 \text{ for } 0 \leq r' \leq N_4 \quad (10)$$

$$0 \leq \rho' \leq 1 \quad (11)$$

While any set of nondimensional parameters will not be unique, this particular choice keeps the bounds simple and minimizes interaction between parameters.

### 3. USING $N_1$ THROUGH $N_4$ DATA FOR OCCULTER DESIGN

One recurring question when contemplating a mission using an occulter is how the properties of a successful occulter would change when the science requirements underlying the design, such as inner working angle or bandpass, are altered. When optimization is used, the effects may not be straightforward to predict *a priori*. However, the parameters  $N_1$  through  $N_4$  are independent and span the space of optimization, and so we can take something of a brute-force approach: create a 4D grid in the four variables and run an optimization at each grid point, giving the worst-case suppression for each  $(N_1, N_2, N_3, N_4)$ . This grid can then be interpolated to provide estimated suppression levels at intermediate points. We define “suppression level” here as the maximum intensity at any point in the occulter shadow and any wavelengths in the occulter bandpass. This is measured at the pupil plane; in many cases, going to an image plane may suppress starlight further at the location of the planet.

Such a grid can be mined for information about the performance and limitations of occulters under various requirements. For example, we can choose a desired suppression level and fix all parameters except for one, for example  $R$ . We would then perform a line search within the  $(N_1, N_2, N_3, N_4)$  space using parameters

$N_1$		$N_2$		$N_3$		$N_4$
26 pts.		12 pts.		9 pts.		10 pts.
7.5		15.0		0.1		0.250
8.0		17.5		0.15		0.306
8.5		20.0		0.2		0.361
9.0		22.5		0.25		0.417
9.5		25.0		0.3		0.472
10.0		27.5		0.35		0.527
10.5		30.0		0.4		0.583
11.0		32.5		0.45		0.638
11.5		35.0		0.5		0.694
12.0		37.5		-		0.750
12.5		40.0		-		-
13.0		42.5		-		-
13.5		-		-		-
14.0		-		-		-
14.5		-		-		-
15.0		-		-		-
15.5		-		-		-
16.0		-		-		-
16.5		-		-		-
17.0		-		-		-
17.5		-		-		-
18.0		-		-		-
18.5		-		-		-
19.0		-		-		-
19.5		-		-		-
20.0		-		-		-

Table 2. Values of  $N_1$ ,  $N_2$ ,  $N_3$ , and  $N_4$  used in the grid.

corresponding to different values of  $R$  to find an  $R$  that matches the our suppression. Repeating this for various wavelength bands will produce minimal occulter sizes to meet performance criteria. (We note that a similar approach for occulter with hypergaussian profiles was undertaken by.<sup>10</sup>) In some cases, swathes may be missing from some plots; these are regions corresponding to points where, for all  $(N_1, N_2, N_3, N_4)$  tabulated, the suppression level is always above or below the desired suppression level, so a transition value cannot be estimated—and corresponding data point—cannot be estimated. These may also be points where there were no  $(N_1, N_2, N_3, N_4)$  values, and more designs would have to be made to fill out these regions.

Our grid consists of 27000 points, with the values of  $N_1$  through  $N_4$  given in Table 2. (There are 28080 possible 4-tuples which can be extracted from these points, but some combinations of these four parameters are excluded for violating the constraint  $N_1 \leq N_2$  implied by the definition in Table 1.)

### 3.1 Data slices and analysis

A common query when considering an occulter is “how big does it have to be?” Occulter size drives occulter mass as the square of the diameter, which in turn drives fuel consumption. Larger occulter must also be further away to maintain the same IWA; this effect goes linearly with diameter. With these considerations in mind, Fig. 2 shows plots of occulter diameter as the shortest and longest wavelengths in the science bandpass are adjusted. All are fixed at  $10^{-10}$  worst-case starlight intensity at the pupil plane across a 6m shadow—a size suitable for finding Earth-like planets with a 4m telescope. The five plots show five values for the geometric (i.e. at the petal tip) IWA: 60mas, 75mas, 90mas, 105mas, 120mas.

The plots in Fig. 2 show the diameter for any potential length of petal (within the extents of  $N_4$ ). However, not all occulter architectures can take arbitrarily-sized petals. For example, the deployment scheme for the  $O_3$  mission concept<sup>11</sup> requires the petals to be wrapped around a central hub, and this wrapped bundle is constrained to be able to fit within a launch fairing. Petal length constraints flow down from this. These properties can be extracted from the data, as well; Fig. 3 shows the bandpass vs. diameter plots redone with a requirement that the petals be 10m long. The colormap is identical in both sets of plots. These additional constraints can increase the total occulter diameter significantly, particularly for occulters with wider bandpasses.

One trend is apparent: increasing the upper wavelength of the bandpass or decreasing the lowest wavelength both require a larger occulter. They are not balanced, however; the rate at which occulter size increases is significantly larger for an increase in wavelength at the upper end of the band. For a fixed petal size, this rate accelerates; the occulter diameter associated with a fixed petal length will always be greater than if the length is allowed to float, but for particularly large bands the discrepancy can be sizable. Consider a 75mas occulter with a 6m shadow, similar to the THEIA mission concept.<sup>3</sup> Bandpasses of 250nm-600nm, 250nm-700nm and 250nm-800nm require occulter sizes of 32.4m, 36.4m and 40.6m, respectively. If the petals are fixed at 10m—the size of the THEIA petals, which were in turn limited by the size of the launch fairing—these increase to 34.6m, 44.2m and 59m: for the larger bands, petal length constraints easily outpace the upper wavelength as the driver of occulter diameter.

A related question starts from the engineering constraints and asks: given an occulter size, and a desired suppression level over a specified shadow, what bandpass and inner working angle are accessible? Fig. 4 shows plots for 4 occulter diameters: 35m, 40m, 45m, and 50m. The same assumptions on shadow and suppression are given as above. An interesting takeaway from these plots is that the inner working angle is very weakly correlated with the lower end of the bandpass, and rather is primarily driven by the longest wavelength. Both views can be combined, as in Fig. 5, which shows contours of IWA as a function of occulter size and distance for the 250nm-600nm, 250nm-700nm and 250nm-800nm bandpasses.

#### 4. SUMMARY

The use of nondimensional parameters in occulter optimizations allow the space of possible occulter designs to be reduced to a minimal, independent set of unitless variables. These can be used to examine the sensitivities of occulter diameter and IWA to variations in bandpass, as well as to span the section of parameter space in which occulters for planet-finding fall.

#### 5. ACKNOWLEDGMENTS

The author would like to acknowledge very fruitful discussions with Stuart Shaklan and Doug Lisman. This work was performed under contract with NASA at the Jet Propulsion Laboratory, California Institute of Technology. Government sponsorship is acknowledged.

#### REFERENCES

- [1] Vanderbei, R., Cady, E., and Kasdin, N., “Optimal occulter design for finding extrasolar planets,” *The Astrophysical Journal* **665**, 794–798 (2007).
- [2] Cady, E., Pueyo, L., Soummer, R., and Kasdin, N. J., “Performance of hybrid occulters using apodized pupil Lyot coronagraphy,” in [*Society of Photo-Optical Instrumentation Engineers (SPIE) Conference Series*], *Society of Photo-Optical Instrumentation Engineers (SPIE) Conference Series* **7010** (Aug. 2008).
- [3] Kasdin, N., Cady, E., Dumont, P., Lisman, P., Shaklan, S., Soummer, R., Spergel, D., and Vanderbei, R., “Occulter design for theia,” *Techniques and Instrumentation for Detection of Exoplanets IV* **7440**(4), SPIE (2009).

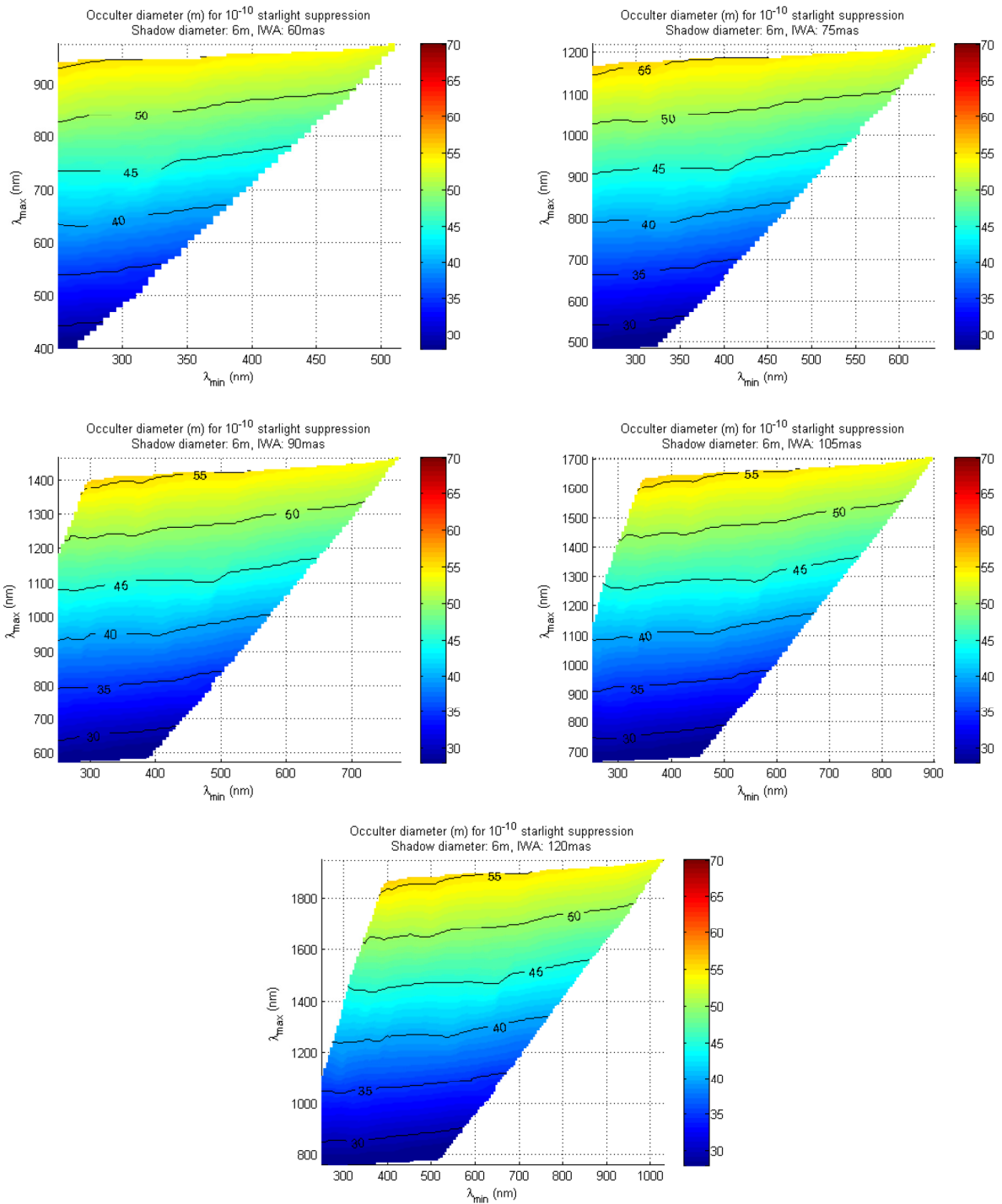


Figure 2. Bandpass versus occulter diameter for a  $10^{-10}$  suppression across a 6m shadow. The shortest wavelength in the bandpass is on the x-axis, and the longest on the y-axis. Contours show lines of constant occulter diameter.

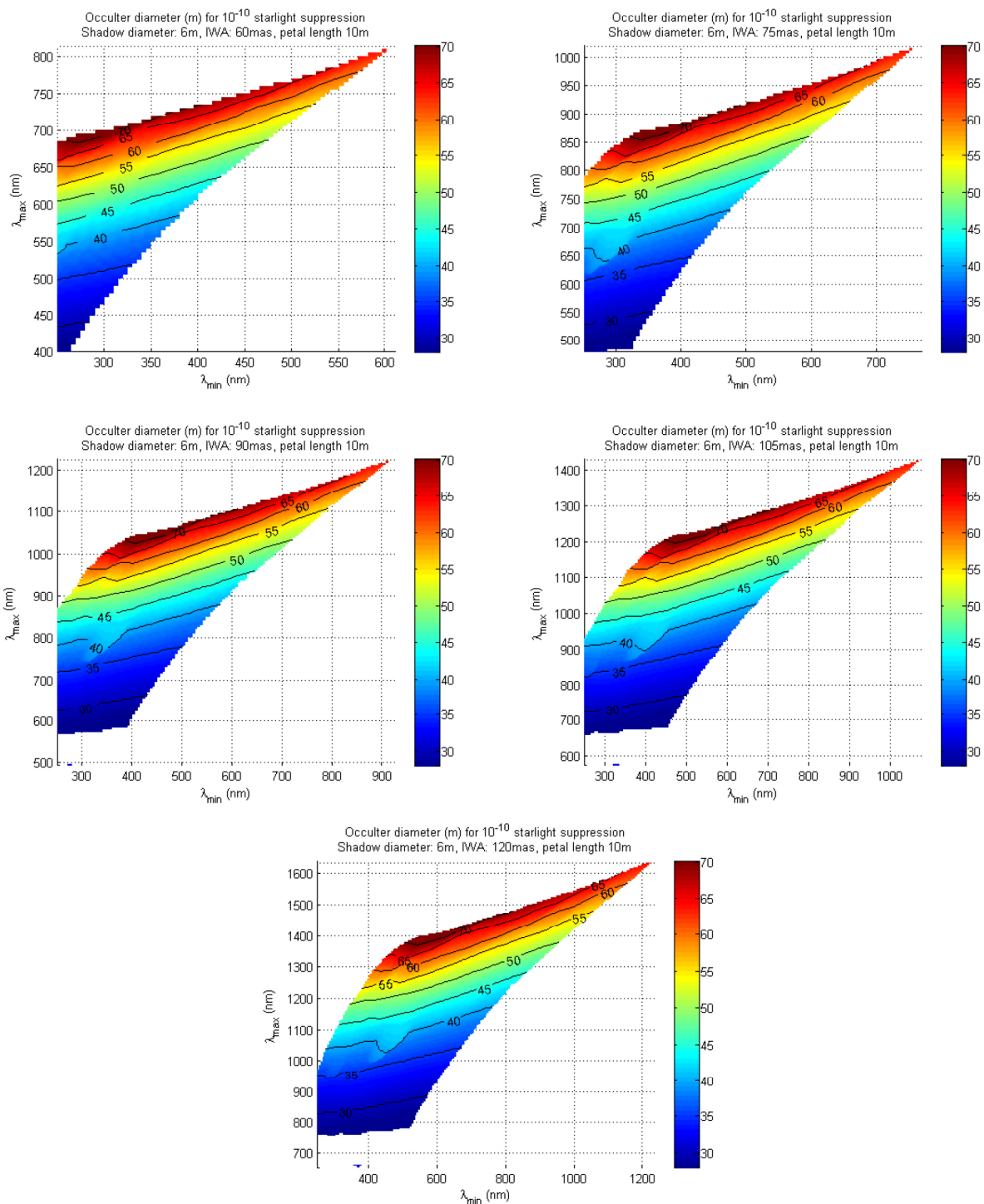


Figure 3. As with Fig. 2, bandpass versus occulter diameter for a  $10^{-10}$  suppression across a 6m shadow. Here the petals are constrained to be 10m long.

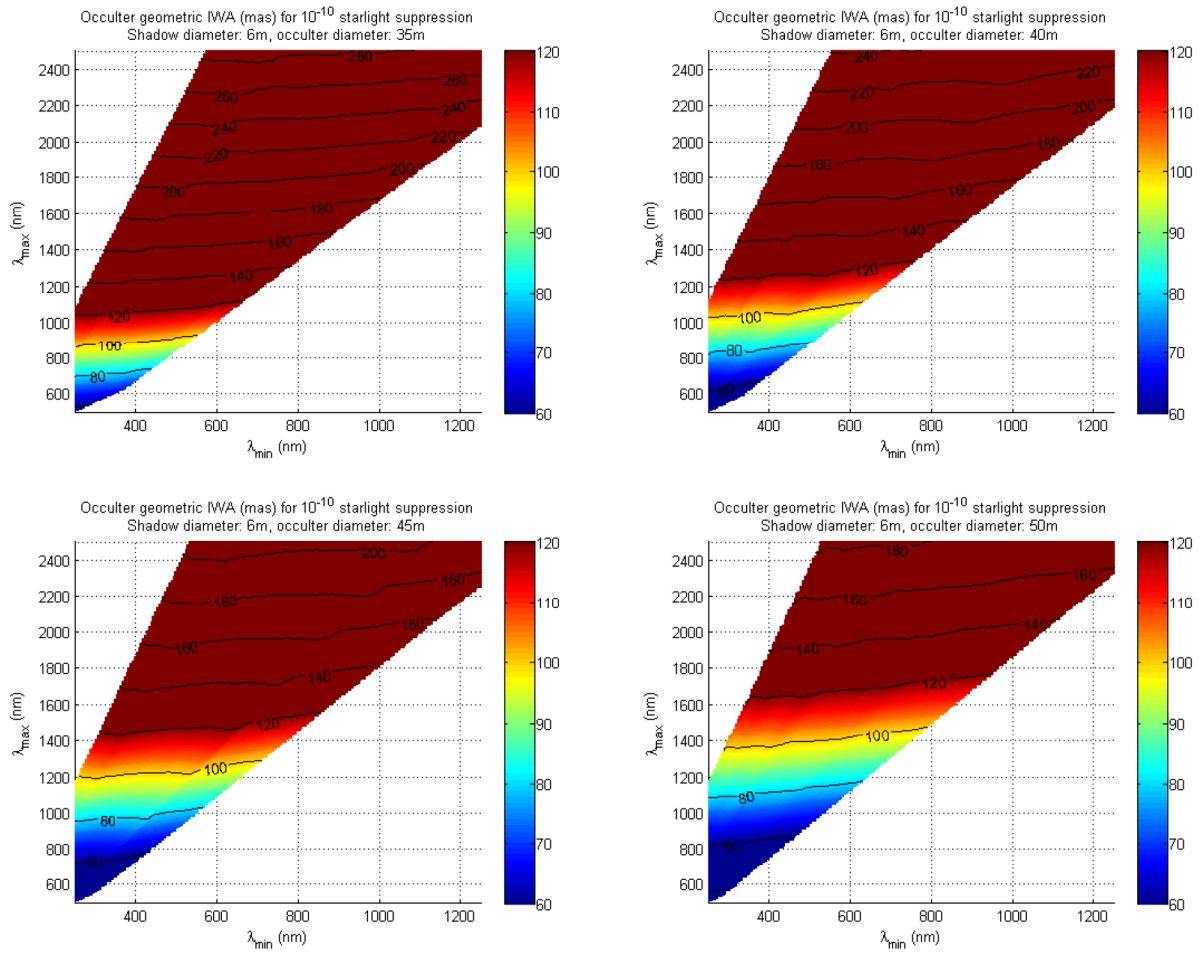


Figure 4. Bandpass versus IWA for a  $10^{-10}$  suppression across a 6m shadow. The shortest wavelength in the bandpass is on the x-axis, and the longest on the y-axis. Contours show lines of constant inner working angle.

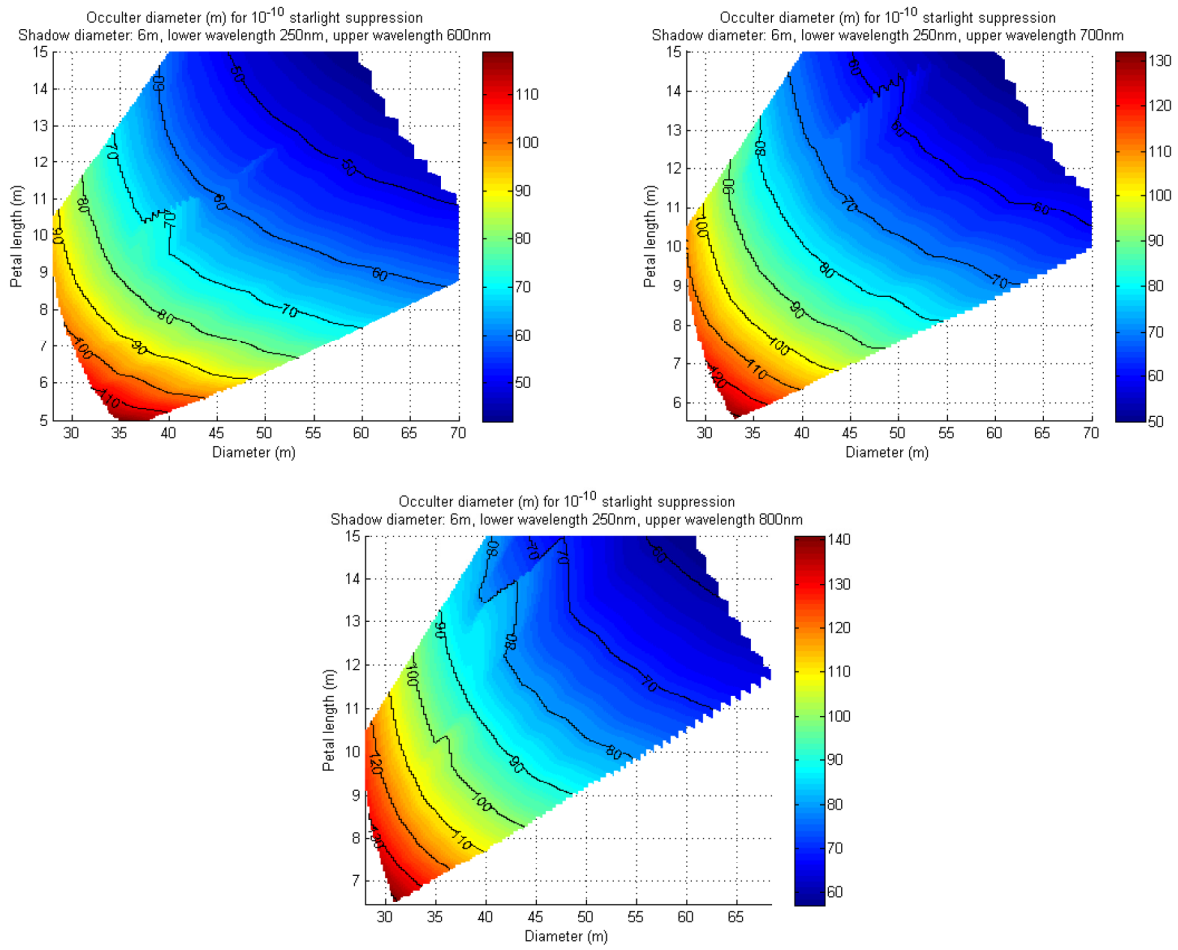


Figure 5. Contours of inner working angle as a function of occulter diameter and petal length, for three UV/visible bandpasses.

- [4] Kasdin, N. J., Spergel, D. N., Lisman, P. D., Shaklan, S. B., Savransky, D., Cady, E., Vanderbei, R., Thomson, M. W., Martin, S. R., Balasubramanian, K., Pravdo, S. H., Sato, Y., and Fujii, Y., “O<sub>3</sub>: The Occulting Ozone Observatory,” in [*Bulletin of the American Astronomical Society*], *Bulletin of the American Astronomical Society* (Jan. 2010).
- [5] Schneider, J., “The extrasolar planets encyclopaedia.” <http://exoplanet.eu> (August 2007).
- [6] Cady, E., Balasubramanian, K., Carr, M., Dickie, M., Echternach, P., Groff, T., Kasdin, J., Laftchiev, C., McElwain, M., Sirbu, D., Vanderbei, R., and White, V., “Progress on the occulter experiment at princeton,” *Techniques and Instrumentation for Detection of Exoplanets IV* **7440**, SPIE (2009).
- [7] Cady, E., Balasubramanian, K., Carr, M., Dickie, M., Echternach, P., Kasdin, J., Shaklan, S., Sirbu, D., and White, V., “Broadband suppression and occulter position sensing at the princeton occulter testbed,” *Space Telescopes and Instrumentation 2010: Optical, Infrared, and Millimeter Wave* **7731**(1), 77312F, SPIE (2010).
- [8] Samuele, R., Glassman, T., Johnson, A. M. J., Varshneya, R., and Shipley, A., “Starlight suppression from the starshade testbed at ngas,” *Techniques and Instrumentation for Detection of Exoplanets IV* **7440**(1), 744004, SPIE (2009).
- [9] Samuele, R., Varshneya, R., Johnson, T. P., Johnson, A. M. F., and Glassman, T., “Progress at the starshade testbed at Northrop Grumman Aerospace Systems: comparisons with computer simulations,” in [*Society of Photo-Optical Instrumentation Engineers (SPIE) Conference Series*], *Presented at the Society of Photo-Optical Instrumentation Engineers (SPIE) Conference* **7731** (July 2010).
- [10] Arenberg, J. W., Lo, A. S., Cash, W., and Polidan, R. S., “New Worlds Occulter performance: a first look,” in [*Society of Photo-Optical Instrumentation Engineers (SPIE) Conference Series*], *Presented at the Society of Photo-Optical Instrumentation Engineers (SPIE) Conference* **6265** (July 2006).
- [11] Savransky, D., Spergel, D. N., Kasdin, N. J., Cady, E. J., Lisman, P. D., Pravdo, S. H., Shaklan, S. B., and Fujii, Y., “Occulting ozone observatory science overview,” *Space Telescopes and Instrumentation 2010: Optical, Infrared, and Millimeter Wave* **7731**(1), 77312H, SPIE (2010).